Supporting Information

Time-dependent Lipid Dynamics, Organization and Peptide-Lipid Interaction in Phospholipid Bilayers with Incorporated β-Amyloid Oligomers

Wei Qiang, Katelynne E. Doherty, Lukas M. Klees, and Yuto Tobin-Miyaji

Department of Chemistry, Binghamton University, State University of New York, Binghamton, New York 13902

Corresponding Author: Dr. Wei Qiang, Email: wqiang@binghamton.edu

S.I. Text

Materials and Methods

Peptide Synthesis. The 40-residue β-amyloid ($A\beta_{40}$) peptides (with or without isotope labeling) were synthesized manually using routine FMOC solid-phase peptide synthesis protocols with Val-preloaded Wang resin (NovaBiochem Inc., 0.2 mmol/g). All crude peptides were cleaved using a cocktail solution containing 82.5% trifluoroacetic acid (*v/v*), 5.0% deionized H_2O (*v/v*), 2.5% phenol (*m/m*), 5.0% thioanisole (*m/m*), 2.5% 1,2-ethanedithiol (1,2-EDT) (*v/v*), 2.5% Me_2S (*v/v*) and 1.5% NH_4I (*m/m*). The peptides were then purified using a reversed-phase HPLC with C18 column (Agilent Inc.), and the mass for all purified peptides were confirmed by LC-MS (Shimadzu Inc.) with purity > 95%. All peptides were lyophilized and stored at -20 °C until usage.

Preparation of Membrane Incorporated $A\beta_{40}$ Oligomers. As sketched in Scheme 1 (main text), the $A\beta_{40}$ peptides and POPC were firstly dissolved in 1.0 mL hexafluoro-isopropanol (HFIP, Sigma-Aldrich Inc.) and 0.5 mL chloroform, respectively. The organic solvents were mixed and removed by N_2 flow, followed by overnight drying under high vacuum. The dried films were resuspended in 20 mM phosphate buffer (pH 7.4, 0.01% NaN_3). The final $A\beta_{40}$ concentration and the final $A\beta_{40}$-to-POPC molar ratio were kept at 200 mM and 1:30, respectively. The aqueous mixture was vortex vigorously at ambient temperature for 10 minutes, followed by 10 freeze-thaw cycles with liquid N_2 and 50-60 °C water bath. The resulted cloudy and homogeneous solution was incubated at 37 °C quiescently for various lengths of time (from zero to four hours in the current work).

The solution was centrifuged after incubation using a Beckmann benchtop Ultracentrifuge (TLA 100.4 rotor, 50,000 rpm, 4°C for 30 minutes, Beckmann Inc.). The pellets were collected and treated with 0.3% (*w/v*) sodium dodecyl sulfate (in deionized H_2O) at ambient temperature for 10 minutes with gentle shaking. No pellet was seen when the resultant transparent solution was centrifuged using the previous ultracentrifugation conditions. Therefore, the solution (~ 1 mL total volume) was centrifuge-filtered using a 30 MWCO filtration Eppendorf centrifuge tube

(Thermo Fisher Inc.) at ambient temperature for 20 minutes. The final sample volume was ~ 10-15 μL and had gel-like morphologies.

Negatively Stained Transmission Electron Microscopy (TEM). The gel-like sample prepared using the protocol above was diluted by 50-fold (*v/v*) using deionized water and a 10 μL drop was deposited on a carbon-coded copper TEM grid (300 mesh, Ted Pella Inc.). The drop was left on grid for 2 minutes for absorption and blot using tissue paper. A 10 μL drop of 2% uranyl acetate was then applied to the grid and left for 30 seconds before blotting. The grid was then rinsed with 10 μL deionized H_2O and dried in the air. The TEM imaging was recorded on a JOEL J-2100 microscope with 80 kV acceleration field. The grid was covered with spherical aggregates as shown in Scheme 1. Images were recorded with 44k X magnification.

Atomic Force Microscopy (AFM). The same gel-like samples were diluted as for the TEM. A 20 μL aliquot were deposit on a fresh mica surface, which were fixed on an AFM magnet disk (Ted Pella Inc.). The solution was kept for 2 minutes before blotting. The surface was then rinsed once with 20 μL 0.1% (v/v) acetic acid to remove the buffer salt, blotted and dried in the air. AFM images were recorded in tapping mode using a Veeco DMASP tips. The typical oscillation frequency, the drive amplitude and the detector set point were kept at 250 kHz, 120-150 mV and ~ 0.6 V, respectively. Images typically contained 256 x 256 points in a 1.5 x 1.5 μm area, scanned at 200 nm/sec rate. Analysis of the height of oligomer were done using ImageJ software for ~ 300 randomly selected species within ~ 15 images (similar to the sample image shown in Scheme 1).

Circular Dichroism (CD) Spectroscopy. The same gel-like samples were diluted by 75-fold using deionized H_2O for CD measurements. The dilution condition was optimized to avoid overwhelming high-tension voltages at low wavelengths. A 300 μL aliquot diluted solution was placed in a quartz cuvette with 1.0 mm pathlength. All spectra were recorded using a JASCO J-810 CD spectrophotometer with temperature controlling at 20°C. Spectra were collected with 40-scan signal averaging from 190 nm to 260 nm. The traces with high-tension voltage > 600 mV were discarded because of the oscillating baselines.

Solid-State Nuclear Magnetic Resonance (ssNMR) Spectroscopy. All ssNMR spectra were recorded on a 600 MHz Bruker spectrometer equipped with a 2.5 mm TriGamma magic-angle spinning (MAS) probe.

The static ^{31}P spectroscopy. The static ^{31}P spectra (Figure 1B) were recorded on samples before the treatment with 0.3% SDS (see the protocol described in the previous section). The purpose was to measure the physicochemical properties of bulk lipid bilayers with incorporated $A\beta_{40}$ oligomers. The samples, after ultracentrifugation, were packed into thin-wall 2.5 mm MAS rotors (~ 15 μL sample volumes) using benchtop Eppendorf centrifuge (500 rpm, 1 minute). All samples were fully hydrated and the ^{1}H signal in H_2O were monitored before and after experiments. Samples were kept at 280 K when spectra were recorded. The static ^{31}P spectra were collected with a simple "direct excitation" pulse sequence (50 kHz ^{31}P $\pi/2$ pulse) with 95

kHz ^{1}H decoupling field through acquisition. Each spectrum was completed with 1024 scans signal-averaging and processed with 200 Hz Gaussian line broadening.

The ^{31}P relaxation spectroscopy and quantitative analysis. The same as static ^{31}P spectroscopy, the ^{31}P relaxation spectra (spin-lattice relaxation, or T_1; and spin-spin relaxation, or T_2) were recorded on samples before the treatment using 0.3% SDS. For both T_1 and T_2 measurements, the MAS frequencies were kept at 10000 ± 2 Hz. The sample temperatures were set as 275K, 285K, 295K and 305K for different experimental sets by measuring the ^{1}H chemical shifts in H_2O.

The T_1 measurements were performed using routine "inversion-recovery" pulse sequence with 55 kHz ^{31}P π and $\pi/2$ pulses and 95 kHz ^{1}H decoupling field. The delay time periods varied from 0.1 ms to 150.1 ms with the increment of 15.0 ms. The T2 measurements were done using routine "Hahn-Echo" pulse sequence with the same ^{31}P and ^{1}H radiofrequency (rf) fields as for T_1. The time delay varied from 0.2 ms to 12.2 ms with the increment of 1.2 ms. Each T1 or T2 data point was recorded with 256 scans signal-averaging.

For quantitative analysis, T_1 and T_2 relaxation spectra were firstly processed with minimum Gaussian line broadening (e.g. 1Hz in Bruker Topspin software) and the peaks were integrated. For both T1 and T2 measurements, the spectral noises were determined as the standard deviations of integrations over 10 arbitrarily picked regions in the corresponding spectra without ^{31}P signals (i.e. noises). The normalized peak volumes *S(t)* versus relaxation times *t* were plotted in Figure 1C-D, and fit to exponential functions, Eqs. S_1 and S_2, for T_1 and T_2, respectively.

$$S(t) = 1 - 2\exp(-\frac{t}{\tau_1}) \text{ (S1)}$$

$$S(t) = \exp(-\frac{t}{\tau_2}) \text{ (S2)}$$

The resultant τ_1 and τ_2 were utilized to calculate R_1 (=1/τ_1) and R2 (=1/τ_2), which were then used in Eqs. 1 and 2 in the main text to solve for the slow-motion and fast-motion correlation times τ_s and τ_f. The temperature-dependence of correlation times were used to calculate the activation energies E_a for the corresponding motions, based on the Arrhenius equation Eq. S3:

$$\ln(\tau) = \frac{E_a}{RT} + C \; where \; \tau = \tau_s \; or \; \tau_f \text{ (S3)}$$

The linear fitting of ln(τ) versus 1/T (temperature in Kelvin) returns E_a. The standard errors of the fitting for E_a were shown in the parentheses in Table S1.

Estimation of the Uncertainties for the Correlation Times. Correlation times (τ_f and τ_s) were obtained by solving the quadratic equations Eqs.1-2 in the main text. Their uncertainties were estimated based on the following derivations.

Two terms contribute to the spin-lattice relaxation rate R_1 and four terms contribute to the spin-spin relaxation rate R_2. Considering the orders of magnitude of τ_s (~ 10^{-9}), τ_f (~10^{-6}) and the values of constants in Eqs. 1-2, the first terms in both R_1 and R_2 are neglectable because they are ~ 10^{-15} while all other terms are between 10^{-8} and 10^{-10}. Furthermore, $(\omega_{31P}\tau_f)^2$ ~ 10 considering the average value of τ_f and constant ω_{31P}. Therefore, the second terms in both R_1 and R_2 are estimated as $\frac{2}{15}\sigma^2\left(1+\frac{\eta^2}{3}\right)(1-S^2)\tau_f^{-1}$ and $\frac{1}{15}\sigma^2\left(1+\frac{\eta^2}{3}\right)(1-S^2)\tau_f^{-1}$ respectively. Eqs. 1-2 in the main text are therefore estimated as:

$$R_1 = \frac{2}{15}\sigma^2\left(1+\frac{\eta^2}{3}\right)(1-S^2)\tau_f^{-1} \quad \text{(S4)}$$

$$R_2 = \frac{1}{15}\sigma^2\left(1+\frac{\eta^2}{3}\right)(1-S^2)\tau_f^{-1} + \frac{4}{45}\omega_{31P}^2\sigma^2\left(1+\frac{\eta^2}{3}\right)\left[s^2\tau_s + (1-S^2)\tau_f\right] \quad \text{(S5)}$$

Error propagations for τ_s and τ_f result in:

$$\sigma_{\tau_f} = \frac{C1}{\omega_{31P}^2}\sigma_{T_1} \quad \text{(S6)}$$

$$\sigma_{\tau_s} = \sqrt{\left(\frac{-C2}{T_2^2}\right)^2\sigma_{T_2}^2 + \left(\frac{C3}{T_1^2} - C4\right)^2\sigma_{T_1}^2} \quad \text{(S7)}$$

, where C1-C4 are constants derived from the 31P Larmor frequency, the CSA, the asymmetric parameter and the order parameters, and their values are 8.74×10^{-9}, 4.29×10^{-9}, 2.20×10^{-9} and 9.58×10^{-8}, respectively. The uncertainties of correlation times are calculated accordingly and reported in Table S1.

The ^{13}C-^{1}H Two-dimensional Wideline-Separation (2D-WISE) Spectroscopy and the estimated order parameter S. The 2D ^{13}C-^{1}H WISE spectroscopy was utilized to estimate the order parameter *S* of the lipid headgroups at different temperatures (from 275 K to 305 K, the same as the ^{31}P relaxation spectroscopy), which was used in the calculations of slow-motion (τ_s) and fast-motion (τ_f) correlation times based on Eqs. 1 and 2 in the main text. Experiments were done with 75 kHz ^{1}H $\pi/2$ *rf* field, followed by 256 t1 increments, 60 kHz ^{1}H cross-polarization (CP) and 50 kHz ^{13}C CP with a linear ramp and 95 kHz ^{1}H decoupling field through acquisition. The MAS frequency was kept at 10000 ± 2 Hz. A representative spectrum at 285 K were shown in Figure S1. All spectra were processed using Bruker Topspin software with 50 Hz Gaussian line broadening in the direct dimension.

The order parameter *S* was estimated from the ^{13}C-^{1}H dipolar coupling splitting (δ_{C-H}) of five lipid phosphate and glycerol carbons that were located close to the headgroup region (Cα, Cβ, C1-3). As shown in the example in Figure S1, the δ_{C-H} values for Cα, Cβ, C1-3 were 3.78, 3.67, 3.73, 4.36 and 3.73 kHz respectively. The rigid limit dipolar coupling strength for a 1.1 Å C-H bond was 22.5 kHz. Therefore, the averaged order parameter S (the ratio between the measured δ_{C-H} and the rigid limit value) was 0.1712 for the example shown in Figure S1. For

different samples, the values were calculated using the same approach and varied between 0.15~0.22.

The ^{1}H-^{1}H NOESY Spectroscopy under MAS. The NOESY spectroscopy was applied to samples before treatments with 0.3% SDS. The sample preparation protocols were the same as described in the previous section with only one modification: the dried lipid/Aβ_{40} films were resuspended in 20 mM phosphate buffer prepared with 95%D_2O/5%H_2O. Because of this modification, the ultracentrifugation was done at 85,000 rpm for 45 minutes (at 4°C) for the increased solvent density. The NOESY spectra were collected with 75 kHz ^{1}H $\pi/2$ *rf* pulses and a series of mixing times from 5 to 750 ms. The sample temperature was kept at 297 ± 2 K based on the monitoring of H_2O ^{1}H chemical shift before and after experiments, and the MAS frequency was 10000 ± 2 Hz. A total 512 t1 points were collected for each mixing time with signal averaging times from 8 to 12 hours. All 2D spectra were processed using nmrDraw software with 10 Hz Gaussian line broadening in both dimensions.

Data analysis was performed to obtain the cross-relaxation rates for H_3C-αH and H_3C-βH interactions (plotted in Fig. 2E of main text). For the quantitative analysis based on Eqs. 3 and 4 in the main text, cross-peak volumes for H_3C-αH, H_3C-βH and diagonal-peak at H_3C-H_3C with different mixing times were integrated and substituted into the left-side of Eqs. 3-4. Both the time-dependent peak volumes for the pair of diagonal/cross-peaks were fit simultaneously to Eqs. 3-4 to obtain the cross-relaxation rates.

The ^{13}C- and ^{31}P-PITHIRDs-CT Spectroscopy and Simulation. The internuclear proximities between selectively labeled ^{13}C sites in Aβ_{40} oligomer or ^{31}P in lipid headgroups were probed using ^{13}C/^{31}P-PITHIRDs-CT pulse sequences. For ^{13}C, the pulse sequence contains a 75 kHz ^{1}H $\pi/2$ pulse, followed by 60 kHz ^{1}H cross-polarization (CP) and 50 kHz ^{13}C CP with a linear ramp and a 33 kHz ^{13}C π-pulse train. The ^{1}H decoupling field was set as 75 kHz during the dipolar evolution time period. The MAS frequency was kept at 20000 ± 2 Hz. For ^{31}P, all parameters were the same as the ^{13}C-PITHIRDs-CT expect that the *rf* field for ^{31}P π-pulse train was set to 37.5 kHz and the MAS frequency was set to 25000 ± 3 Hz. The pulsed-spin locking scheme, which refocused the anisotropy effects. Was applied during acquisition to enhance the resonance peak intensities.

For data analysis, the peak volumes were obtained from integration and the normalized volumes were plotted versus the dephasing time (Fig. 3B and Fig. 4A-C in the main text). The noise of a spectrum was determined by calculating the standard deviations of integrations over the same range as the peak around 10 randomly selected baseline positions. These noises levels were plotted as error bars in Fig. 3B and Fig. 4A-C. Simulation of PITHIRDs-CT experiments were performed using SIMPSON package. For ^{31}P, the model system contained four ^{31}P nuclei arranged in a square (Fig. 3A in the main text). For ^{13}C (Fig. S3), the model system contained three ^{13}C nuclei arrange linearly to mimic the alignment of specific labeled sites in the parallel-in-register β sheet structures.

The ^{13}C-^{31}P REDOR Spectroscopy and Simulation. The REDOR pulse sequences (^{13}C- or ^{31}P-detected) contained a 75 kHz ^{1}H $\pi/2$ pulse, followed by 60 kHz ^{1}H cross-polarization (CP) and 50 kHz ^{13}C CP with a linear ramp, rotor synchronized ^{13}C and/or ^{31}P π-pulse trains with 50 kHz and 55 kHz rf fields respectively. A 95 kHz ^{1}H decoupling field was applied during the dipolar evolution time period. The pulsed-spin locking schemes were applied during acquisition. The MAS frequency was kept at 8000 ± 2 Hz and the sample temperature was kept at 295 K by monitoring the ^{1}H chemical shifts in H_2O.

For data analysis shown in Fig. 3D and Fig. 4G-I, integrations were done for S_0 (with ^{13}C-^{31}P dipolar coupling averaged to zero) and S_1 (with ^{13}C-^{31}P dipolar coupling recovered) over 0.5 ppm around the peaks. The dephasing was quantified as $(S_0 - S_1)/S_0$. The error bars consider the noise levels in both S_0 and S_1 spectra. Standard deviations of S_0 and S_1 spectral noises, σ_{S_0} and σ_{S_1} respectively, were obtained by integrating 10 randomly selected 0.5 ppm regions without signals. The error bars of REDOR dephasing were then calculated using:

$$\sigma\left(\frac{\Delta S}{S_0}\right) = \sqrt{S_1^2\sigma_{S_0}^2 + S_0^2\sigma_{S_1}^2}/S_0^2 \text{ (S8)}$$

Fitting of REDOR data (dephasing versus dipolar evolution times) was done using a two-spin ^{13}C-^{31}P model system, with two fitting parameters: a best-fit ^{13}C-^{31}P internuclear distance (*r*) and a population weighing factor (*A*). The theoretical ^{13}C-^{31}P dephasing curve was calculated based on Eq. S9 given by literature:

$$\left(\frac{\Delta S}{S_0}\right)^{sim}(t) = A[1 - \{J_0[\sqrt{2}t\left(\frac{23.05}{r}\right]^3\right]]^2 + 2 \times \sum_{k=1}^{5} \frac{\{J_k[\sqrt{2}t\left(\frac{23.05}{r}\right]^3\right]]^2}{16k^2 - 1}] \text{ (S9)}$$

, where t was the dipolar evolution time and J represented the BesselJ function. The experimental REDOR dephasing $\left(\frac{\Delta S}{S_0}\right)^{exp}$ values with different dipolar evolution times were fit to the simulated values to minimize the deviation, which as defined as:

$$\chi^2 = \sum_i \frac{[\left(\frac{\Delta S}{S_0}\right)_i^{exp} - \left(\frac{\Delta S}{S_0}\right)_i^{sim}]^2}{[\sigma\left(\frac{\Delta S}{S_0}\right)]^2} \text{ (S10)}$$

, where i is the number of dephasing times taken in experiments. Figure S4 and Table S2 summarize the fitting results for experiments with $\left(\frac{\Delta S}{S_0}\right)^{exp}$ > 0.1 at 22.4 ms. The best-fit populations and distances were obtained when the deviation reach minima (i.e. χ^2_{min}) and their uncertainties were determined using the criterion $\chi^2 = \chi^2_{min} + 1$.

S.I. Tables

Table S1. Summary of quantitative analysis of ^{31}P relaxation spectroscopy

Incubation Time (hours)	initial		1.0		2.0		3.0		4.0	
	τ_f (ns)	τ_s (μs)	τ_f (ns)	τ_s (μs)	τ_f (ns)	τ_s (μs)	τ_f (ns)	τ_s (μs)	τ_f (ns)	τ_s (μs)
275 K	1.45 (0.06)	2.24 (0.16)	1.63 (0.06)	0.79 (0.05)	1.62 (0.07)	0.95 (0.05)	1.70 (0.07)	0.97 (0.05)	1.40 (0.06)	2.25 (0.08)
285 K	1.42 (0.06)	2.10 (0.16)	1.43 (0.06)	0.74 (0.05)	1.38 (0.07)	0.76 (0.05)	1.49 (0.06)	0.72 (0.04)	1.32 (0.06)	1.97 (0.13)
295 K	1.39 (0.06)	1.95 (0.18)	1.25 (0.06)	0.56 (0.05)	1.18 (0.06)	0.73 (0.05)	1.47 (0.06)	0.68 (0.05)	1.30 (0.06)	1.68 (0.17)
305 K	1.37 (0.06)	1.83 (0.21)	1.02 (0.06)	0.54 (0.05)	0.79 (0.05)	0.69 (0.07)	1.36 (0.06)	0.68 (0.07)	1.23 (0.06)	1.35 (0.21)
Activation Energy (kJ/mol)	1.0 (0.2)	6.6 (0.9)	10.7 (1.1)	9.9 (2.2)	16.0 (3.2)	7.0 (1.9)	4.8 (1.0)	8.0 (3.2)	6.4 (2.4)	13.3 (2.1)

Table S2. Summary of ^{13}C-^{31}P REDOR fitting based on Eq. S5

Residue	Incubation Time (hours)	Best-fit Population	Best-fit Distances (Å)
V36	3.0	0.08(0.01)	6.3(0.2)
	4.0	0.14(0.02)	6.3(0.2)
G25	2.0	0.10(0.01)	5.9(0.2)
	3.0	0.14(0.02)	5.7(0.1)
	4.0	0.26(0.03)	5.7(0.1)

S.I. Figures

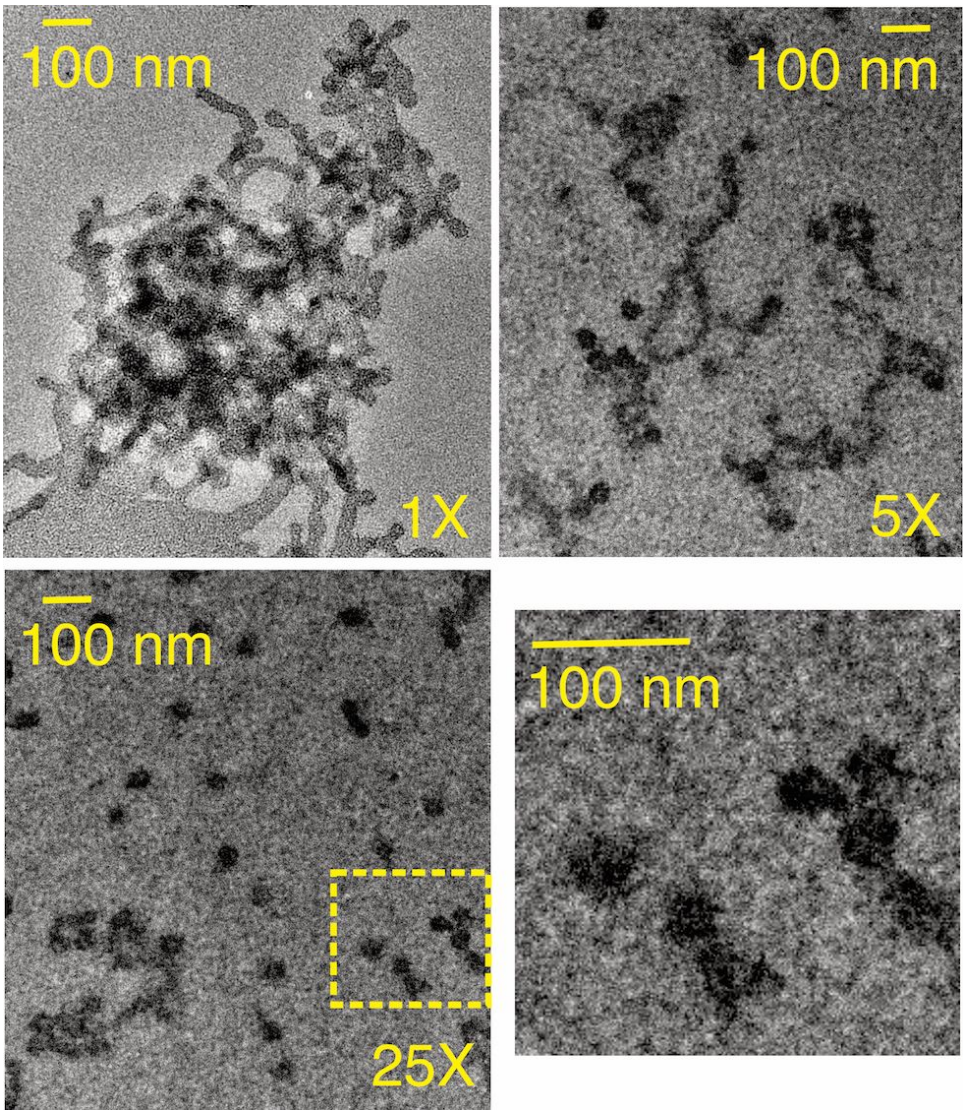

Figure S1: Negatively stained TEM images for the series-diluted oligomer samples prepared using the protocols shown in Scheme 1. The spherical oligomers were visualized at all concentrations. At higher concentrations, however, the oligomers showed higher tendency to form amorphous and/or curvy filament-like morphologies.

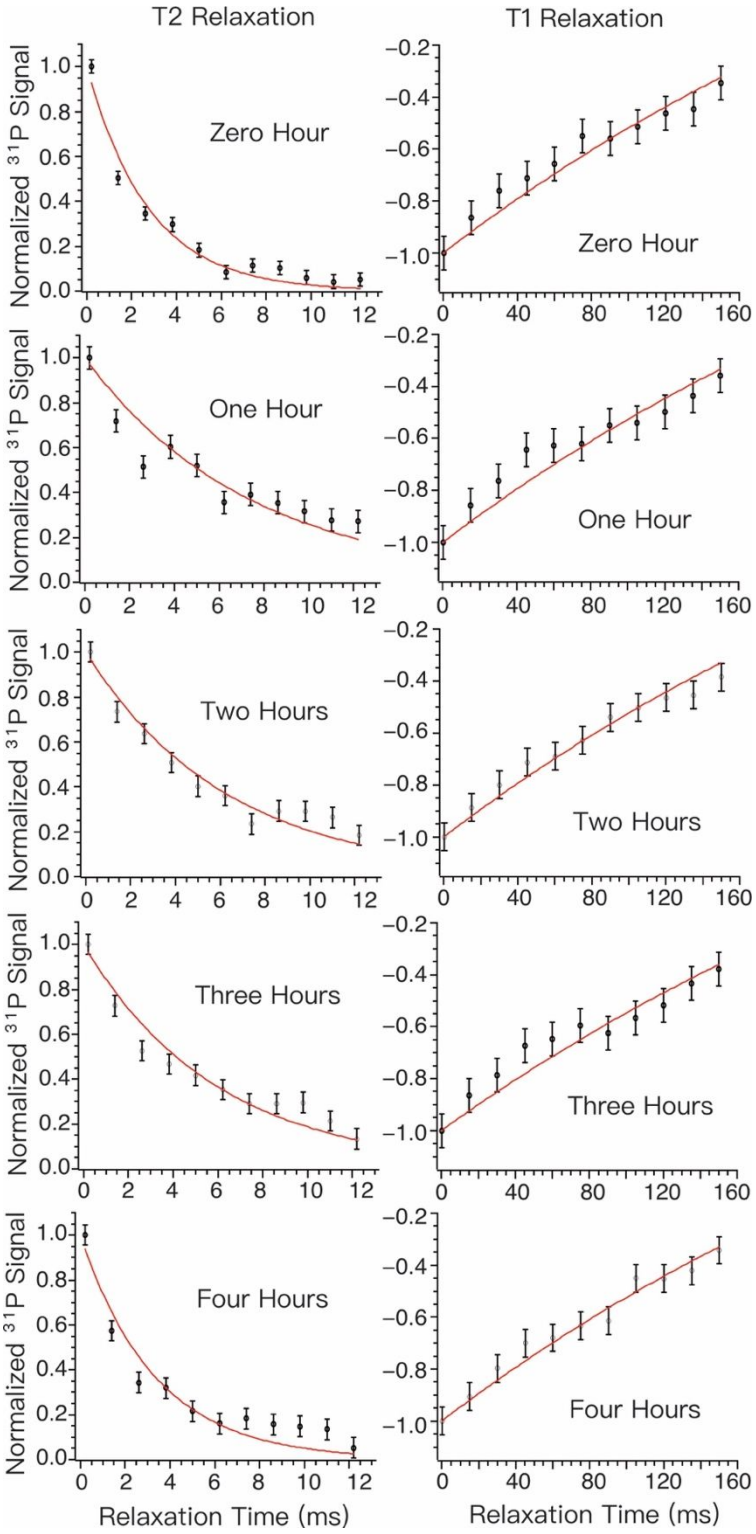

Figure S2: Representative fitting for the T_1 and T_2 relaxation measurements (275K, the same experimental data shown in Fig. 1C-D). The experimental data were shown in black symbols with error bars and the fitting to Eqs. S1-2 were shown in red lines.

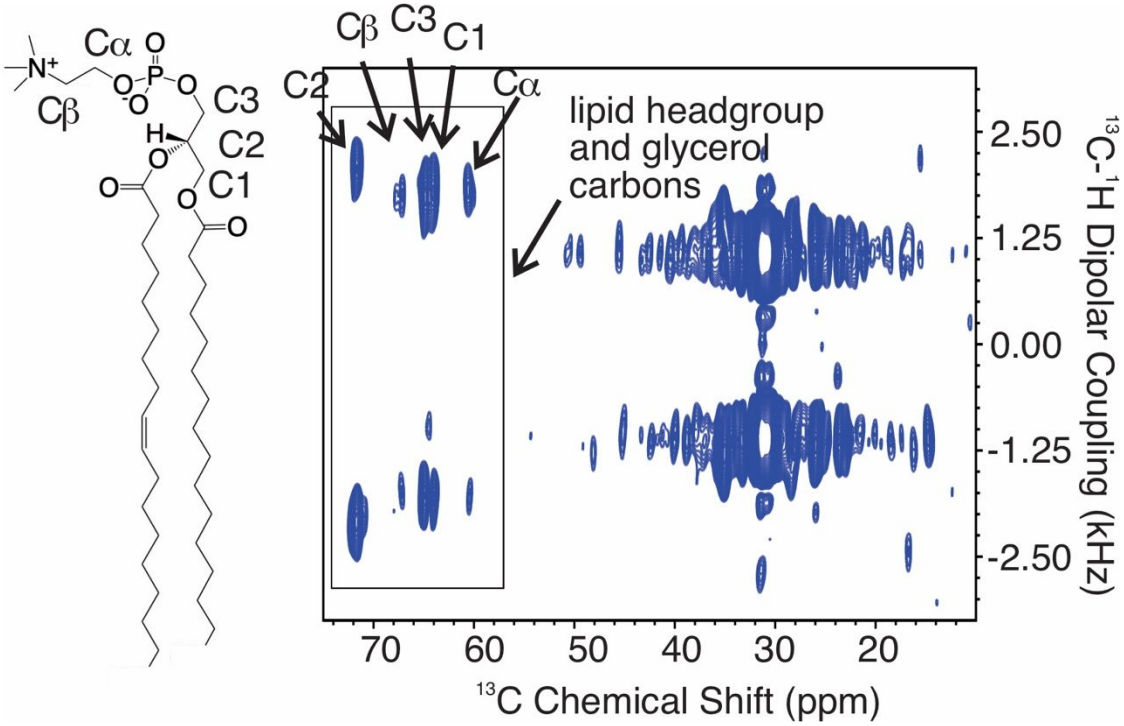

Figure S3: A representative 2D ^{13}C-^{1}H WISE spectrum (collected at 285K for the sample with one-hour incubation time). Estimation of the lipid headgroup order parameter *S* considered five lipid phosphate group and glycerol carbons (Cα, Cβ and C1-3), labeled on the chemical structure of POPC (left side). The rigid limit dipolar coupling for a 1.1 Å C-H bond was 22.5 kHz.

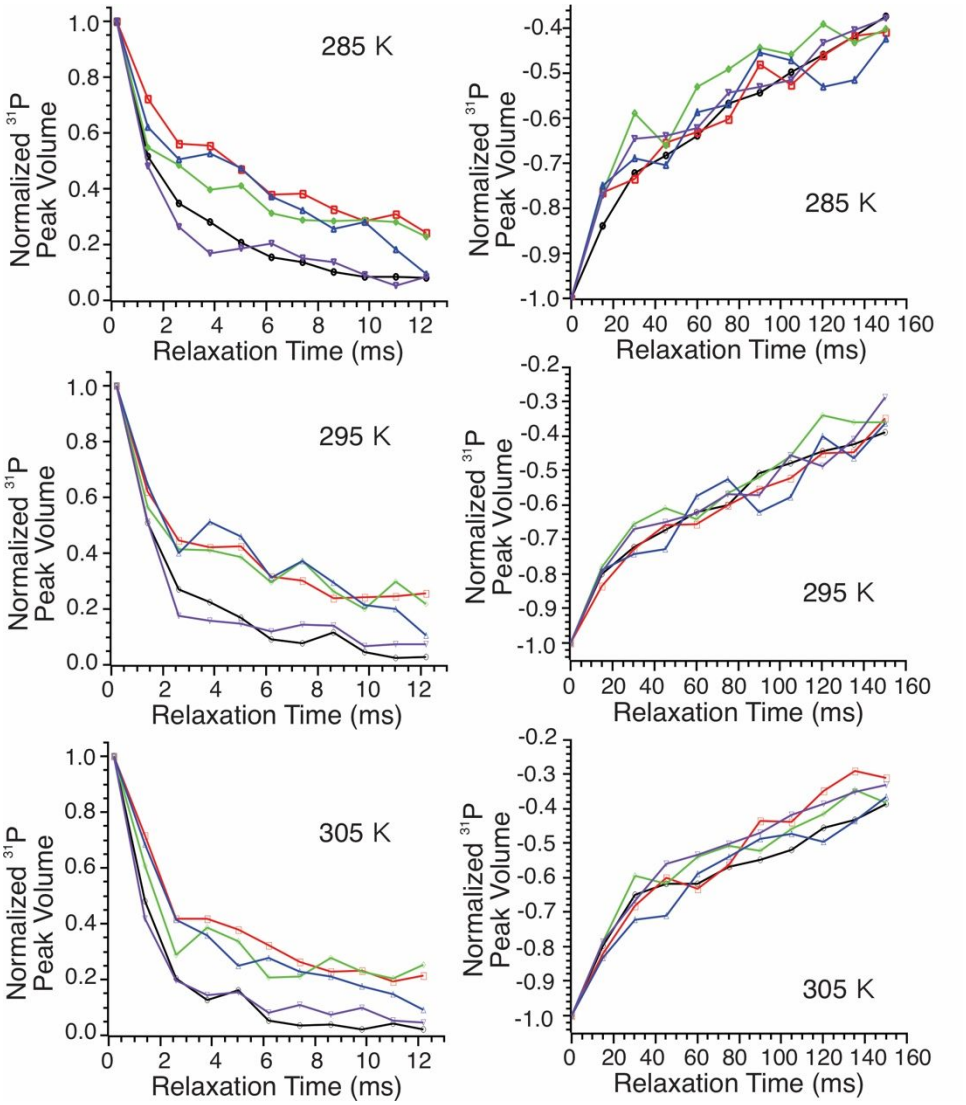

Figure S4: ^{31}P relaxation curves (T2, left side; T1, right side) for POPC bilayers with incorporated $A\beta_{40}$ oligomers recorded at different temperatures (285K, 295K and 305K). Color-coding used for samples with different incubation times: black, zero; red, one hour; green, two hours; blue, three hours; purple, four hours.

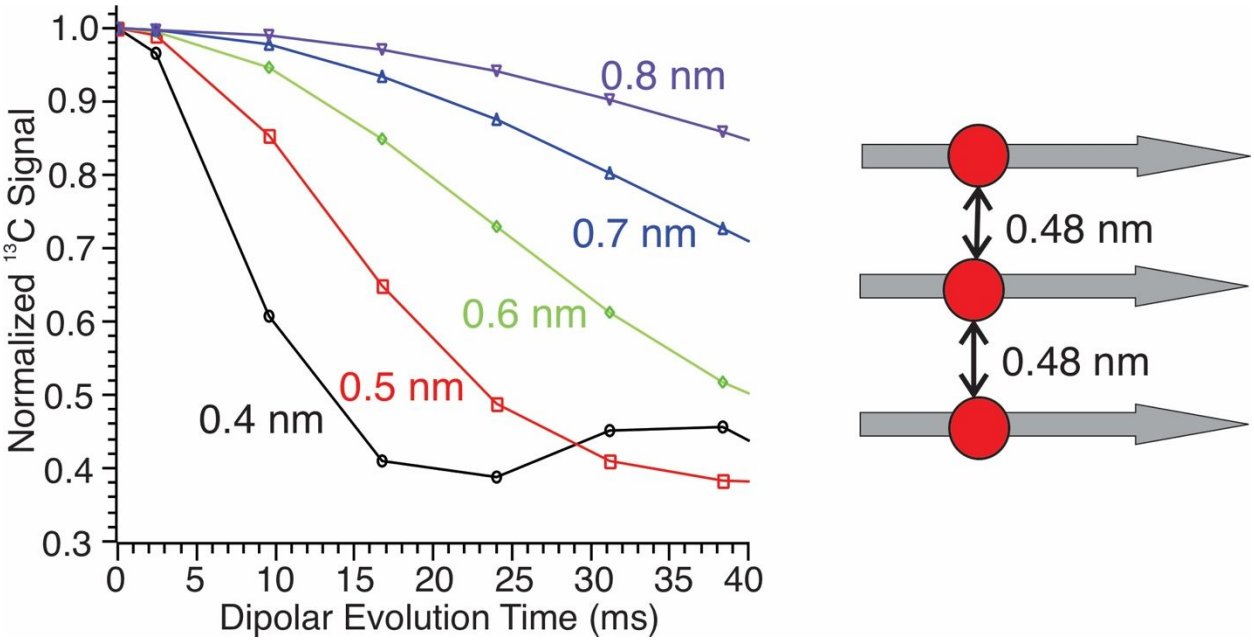

Figure S5: Simulated ^{13}C-PITHIRDs-CT dephasing curves for a three-spin model in a parallel-β-sheet (right side) with different internuclear distances from 0.4 to 0.8 nm. Simulation was done by SIMPSON software. Experimental data shown in Figure 4A-C (main text) fit between 0.5 to 0.7 nm, depending on the labeling sites and different incubation times.

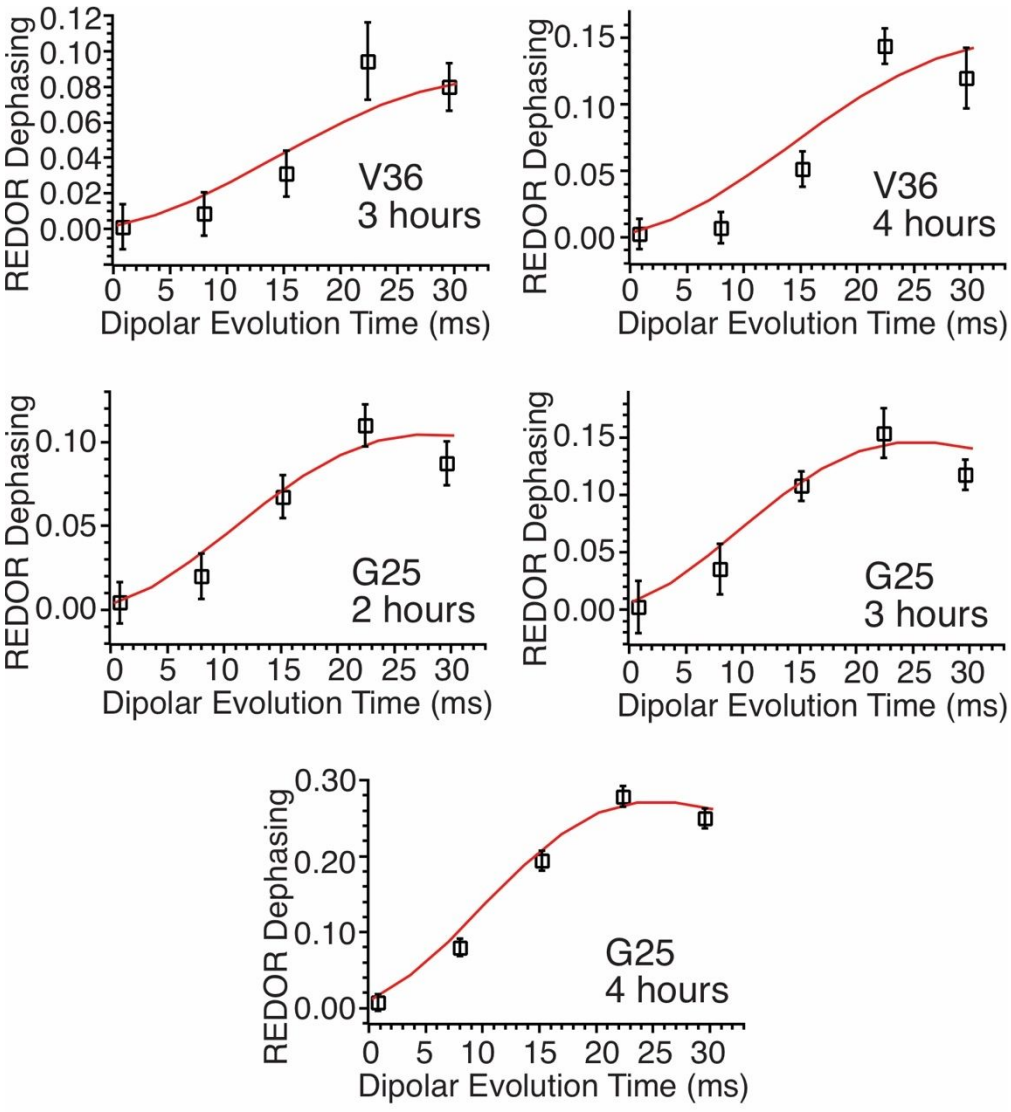

Figure S6: Fitting of the experimental ^{13}C-^{31}P REDOR dephasing (Figure 4G-I, main text) to a two-spin ^{13}C-^{31}P model (Eqs. S8-9). The experimental data was shown in open symbols and the simulated curves were shown in red. The fitting results (best-fit populations and internuclear distances) were shown in Table S2.